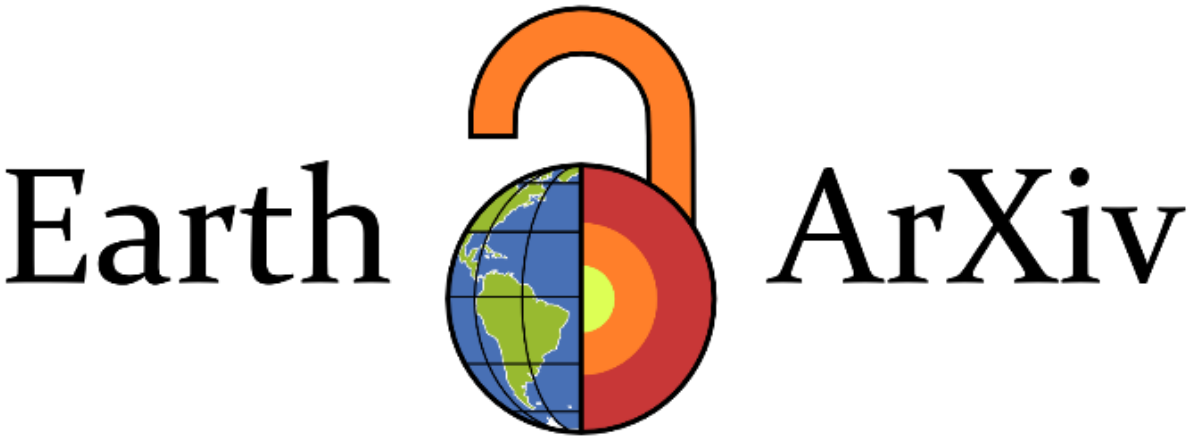

Xerokampos: Evidence for a localized hot desert microclimate enclave

Chatzopoulos Iasonas[1,*], Stavrakakis Nikolaos[2]

[1] Independent Researcher, Athens, Greece

[2] Independent Researcher, Heraklion, Greece

Abstract

This study investigates the spatial precipitation distribution and microclimatic characteristics of the coastal enclave of Xerokampos, Lasithi in Greece. Utilizing a local meteorological time series (2020-2026), the mean annual precipitation (MAP) is recorded at 219.5 mm, alongside a mean annual temperature of 20.9°C. To contextualize these limited contemporary observations, a synthetic climate reconstruction (1915-1929) and a 30-year ERA5 marine reanalysis (1996-2026) were applied, yielding MAP estimates of 171.2 mm and 227.1 mm, respectively. The region's aridity is quantified using multiple bioclimatic indices. The United Nations Environment Programme (UNEP) Aridity Index yields values of 0.178 (Holdridge) and 0.199 (Thornthwaite), both falling within the desert regime (< 0.20). Additionally, the De Martonne Aridity Index ranges between 5.54 (synthetic) and 7.10 (contemporary), while the Köppen-Geiger desertification threshold is calculated at 209.0 mm. This persistent precipitation deficit is primarily driven by the rain shadow effect and dry adiabatic heating (Foehn effect) induced by the adjacent Ziros massif. Furthermore, the local bioclimatic stress is corroborated by the Sitia UNESCO Global Geopark, which classifies the coastal zone as semi-desert, hosting unique North African thermophilic flora. Integrating thermodynamic modeling with empirical indices, findings suggest that Xerokampos likely constitutes a structurally localized Hot Desert (Köppen: BWh) microclimate enclave.

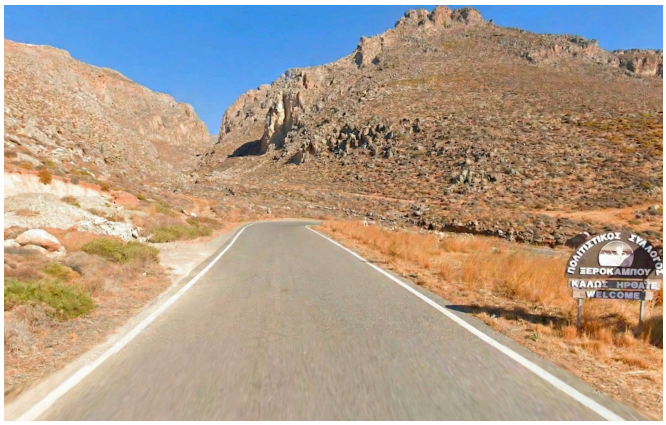

Figure 1: Characteristic view of the arid entrance to Xerokampos, Lasithi, where desert vegetation and bare soil dominate.

[0]*ORCID: https://orcid.org/0009-0008-5848-2360, Corresponding author. E-mail address: xerokamposdesertresearch@outlook.com

1 Introduction

The Mediterranean basin is characterized by high spatial and temporal variability regarding precipitation distribution, making it one of the most prominent climate change hotspots globally (Nastos & Zerefos, 2009; Lionello et al., 2006). Over the past decades, shifting synoptic circulation patterns have progressively exacerbated the vulnerability of the eastern Mediterranean to prolonged dry spells and desertification processes. In the southeastern tip of Greece, eastern Crete has been historically recognized as a zone of acute climatic aridity (Flocas & Bloutsos, 1991). As early as the beginning of the 20th century, Mariolopoulos (1938) classified the area east of Ierapetra into the **Desert-like Mediterranean climate** (207.1 mm), a pioneering observation that laid the groundwork for contemporary microclimatic investigations. Modern analyses robustly confirm a persistent trend of localized water resource depletion, driven by both decreasing precipitation totals and increasing atmospheric evaporative demand (Tsanis et al., 2011; Vrochidou et al., 2013).

Within this broader macro-climatic context, the coastal strip of Xerokampos, Lasithi constitutes an extreme topographical and bioclimatic anomaly. Coastal microclimates in complex topographies often deviate significantly from regional interpolations, largely due to intense land-sea boundary layer interactions and abrupt orographic forcing (Mass et al., 2002; Warner, 2010). The etymology of the toponym itself ("xeros" meaning dry and "kampos" meaning plain) acts as a historical proxy record, indicating that the lack of water resources is a structural, long-term characteristic of the area deeply embedded in local geography (Demetrakos, 1950).

The profoundly arid physiognomy of the landscape is concurrently supported by the unique floristic composition of the area. The geographical proximity to North Africa, combined with the severe precipitation deficit, allows the survival and propagation of specialized thermophilic and drought-resistant flora that cannot easily establish elsewhere in the Aegean. This dynamic is corroborated by the Sitia UNESCO Global Geopark (2026), which encompasses the broader southeastern coastal zone, including Xerokampos and the adjacent Koufonisi islet. The Geopark formally characterizes this coastal enclave as "semi-desert" and reports that it hosts North African plant species that are entirely unique within the Greek territory.

Specifically, the presence of thermophilic and desert taxa in this localized ecosystem acts as a highly reliable bio-indicator of extreme xerothermic conditions. Key species include the African *Ziziphus lotus* (a thorny shrub with profound drought tolerance, notably abundant on the immediately adjacent Koufonisi), the Saharo-Arabian grass *Lygeum spartum*, and the peri-Saharan *Periploca angustifolia* (Municipality of Sitia, 2024).

The ecophysiological adaptations of these species—such as extensive root networks capable of exploiting deep moisture reserves, reduced leaf surface areas, and thick waxy cuticles to minimize transpiration—reflect a profound evolutionary response to severe environmental stress (Rackham & Moody, 1996; Turland et al., 1993). The dominance and sustained prevalence of such adaptations strongly indicate the continuous, structural stress of the ecosystem stemming from a permanent precipitation deficit (Eig, 1931).

Furthermore, it is noteworthy that the survival of these North African taxa is synergistically supported by highly specialized local edaphic conditions. The sandy, skeletal, and saline soils characterizing the Alatsolimni (salt lake) ecosystem of Xerokampos (Municipality of Sitia, 2024) act as an environmental filter. This saline substrate mimics the harsh conditions of North African chotts and sebkhas, providing a unique ecological niche that further differentiates the microclimate from the typical Mediterranean sclerophyllous environment. The convergence of topographical shielding, high insolation, minimal precipitation, and saline soils creates a highly specific biome. Despite visual and biological indications of its desert-like nature, this enclave has largely evaded quantitative climatological categorization due to the historical absence of high-resolution in-situ monitoring networks. This study provides, to our knowledge, the first rigorous mathematical and quantitative evidence for a persistent rain-shadow desert microclimate in Greece, establishing a baseline for future micro-meteorological research.

2 Data and Mathematical Methodology

The research is based on the analysis of three meteorological time series. Specifically, for Xerokampos, secondary data were extracted from the local meteorological station (Davis type, 8 m) (Xerokampos Weather Station, 2026), which are compared with the NOA (2026) stations in Ierapetra (15 m, 2007-2026) and Toplou Monastery (170 m, 2019-2026) (Kotroni et al., 2020). The Xerokampos in-situ dataset is used solely for scientific analysis under academic fair-use conditions. The data are employed for non-commercial research purposes with full attribution to the original provider and are not redistributed in raw form. All statistical processing is performed on derived aggregates (monthly and annual values), ensuring compliance with data usage restrictions specified by the source. This study does not claim ownership of the original measurements. The following 6 mathematical criteria were applied:

1. Köppen-Geiger Criterion (Desertification Threshold) (Beck et al., 2023):
Adjusted for Mediterranean precipitation seasonality ($> 70\%$ occurring in winter), the Hot Desert (BWh) threshold is defined as:

$$P_{\text{threshold (BWh)}} = 10 \times T_{\text{mean}}(^{\circ}\text{C}) \tag{1}$$

2. UNEP Aridity Index:

$$AI = P_{\text{annual}}/PET \tag{2}$$

3. Rain Shadow Ratio (RSR):

$$RSR = \frac{\Sigma P_{\text{Xerokampos}}}{\Sigma P_{\text{Ierapetra}}} \tag{3}$$

4. Historical Precipitation Estimation:

$$P_{\text{Hist\_Xero}} = P_{\text{Hist\_Iera}} \times RSR \tag{4}$$

5. Holdridge Life Zone System (Holdridge, 1947; 1967):

$$PET \approx 58.93 \times BT \tag{5}$$

6. De Martonne Aridity Index (De Martonne, 1926):

$$I = P_{\text{annual}}/(T_{\text{mean}} + 10) \tag{6}$$

3 Results

3.1 Precipitation and General Climatology

The spatial differentiation of precipitation in the extreme southeast of Crete proves to be exceedingly rapid and topographically dependent. The reference stations on the windward or unshielded exposures report significantly higher moisture inputs: Toplou Monastery, located to the north, records an average of 337.2 mm, while Ierapetra, further west along the southern coast, records 363.2 mm. In stark contrast, the shielded coastal enclave of Xerokampos records a mere 219.5 mm over the contemporary observation period. This abrupt gradient highlights the severe impact of local topography on synoptic weather systems traversing the island.

Table 1: Comparative Table of Mean Monthly Precipitation (mm)

Station	Jan	Feb	Mar	Apr	May	Jun	Jul	Aug	Sep	Oct	Nov	Dec	Total
Xerokampos (2020-2026)	49.0	39.2	29.6	7.6	5.4	5.5	0.3	0.7	2.6	21.6	18.5	39.5	**219.5**
E. Ierapetra (1915-1929)	52.3	28.8	17.3	8.2	4.4	6.0	0.0	0.0	5.1	14.1	31.2	39.7	**207.1**

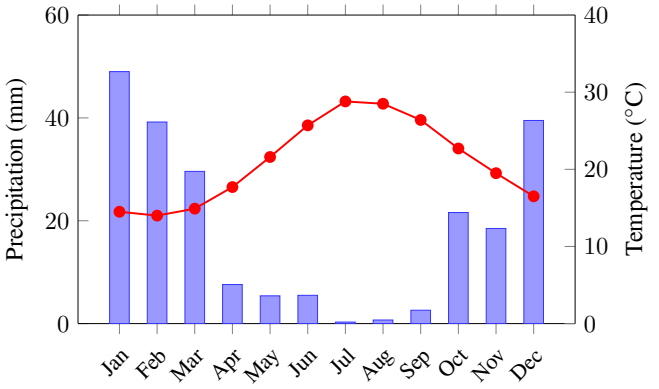

Figure 2: Xerokampos Lasithi Climograph (2020-2026). Depiction of the profound xerothermic period.

3.2 Temperature Regime and Thermal Stress

Beyond the severe lack of precipitation, Xerokampos distinguishes itself as the warmest enclave within the broader study zone, registering a remarkable mean annual temperature (T_{mean}) of 20.9°C. This thermal anomaly is intrinsically linked to its geographical position, southerly exposure, and the localized thermodynamic warming caused by descending winds. The temperature profile is characterized by exceptionally mild winters and

prolonged, intense summers. Absolute minimum temperatures do not fall below 3.8°C, with the mean of absolute minimums at 5.6°C, effectively eliminating the incidence of frost. This thermal stability classifies the area securely within the USDA 11a plant hardiness zone (Magarey et al., 2008), a critical environmental prerequisite that explains the unhindered proliferation of frost-intolerant North African taxa.

During the prolonged xerothermic period (extending from April to October, as illustrated in the climograph), diurnal temperature ranges are amplified by the low atmospheric humidity and clear skies, which maximize incident solar radiation. The summer boundary layer is frequently dominated by extremely warm and dry continental air masses originating from North Africa, further exacerbated by local adiabatic heating when northern flow (Meltemi) is forced over the Cretan mountains. This persistent thermal stress, coupled with near-zero summer precipitation, generates an extreme vapor pressure deficit (VPD) that dictates the harsh ecological boundaries of the local biome.

To extract the deep historical background and normalize the brief contemporary data, the baseline ratio $RSR = 0.718$ was calculated against the nearest long-term historical station.

Table 2: Synthetic Climate Reconstruction Model (1915-2026)

Period	Base Precipitation	RSR	Estimated Precipitation
Historical (1915-1929)	207.1 mm	0.718	**148.7 mm** (n=15 yrs)
Contemporary (2020-2026)	-	-	**219.5 mm** (n=7 yrs)
Synthetic Avg.	-	-	**171.2 mm** (n=22 yrs)

4 Discussion and Thermodynamic Analysis

4.1 Thermodynamics of the Katabatic Foehn Winds

The persistent precipitation deficit observed in Xerokampos cannot be explained solely by broader regional trends; it is inextricably linked to the localized thermodynamics of the Foehn phenomenon. The Ziros mountain massif (averaging 800 meters in elevation) acts as an impenetrable orographic barrier to the prevailing northerly and northwesterly synoptic flows.

When moisture-laden air masses approach from the Aegean Sea, they are forced to ascend the windward slopes of the massif. This mechanical lifting causes the air to cool at the saturated adiabatic lapse rate, leading to condensation and enhanced orographic precipitation on the northern, windward side (e.g., Toplou Monastery). Having depleted a significant portion of their moisture content, these air masses then crest the plateau and begin their descent toward the Libyan Sea on the leeward side.

Descending on the leeward side, the now-dry air masses undergo severe compression and heat up according to the Dry Adiabatic Lapse Rate:

$$\Gamma_d = \frac{g}{c_p} \approx 9.8^{\circ}\text{C/km} \tag{7}$$

This rapid, sensible heat flux drastically reduces the relative humidity of the descending air. The primary meteorological consequence is the enhanced sub-cloud evaporation of hydrometeors (virga). As precipitation falls from the mid-level clouds generated over the peaks, it encounters this aggressively hot and dry boundary layer over Xerokampos. The vertical raindrops evaporate in mid-air before ever reaching the ground, effectively nullifying the rainfall potential of the passing weather system. This constant thermodynamic suppression is the primary driver of the enclave's aridity.

The application of the Holdridge method to quantify the resulting evaporative demand yields:

$$PET_{\text{Holdridge}} = 58.93 \times 20.9 = 1,231.6\,\text{mm} \quad (AI = 0.178) \tag{8}$$

While the Thornthwaite method is calculated respectively at:

$$\begin{aligned} PET_{\text{Thornthwaite}} &= \sum_{i=1}^{12} 16 \left(\frac{10 \cdot T_i}{I} \right)^a \\ &= 1,100.5\,\text{mm} \quad (AI = 0.199) \end{aligned} \tag{9}$$

These values indicate the enclave marginally satisfying the absolute Arid regime threshold, reflecting a severe imbalance between moisture input and atmospheric demand.

4.2 Methodological Considerations on Evapotranspiration

A recognized limitation of this macro-climatic study is the reliance on temperature-based empirical models (Holdridge, Thornthwaite) for estimating Potential Evapotranspiration (PET), rather than the physically-based FAO-56 Penman-Monteith equation. The Penman-Monteith methodology is globally acknowledged as the gold standard, as it incorporates a comprehensive suite of aerodynamic and radiation parameters. However, it requires continuous, high-fidelity historical datasets of solar radiation (R_s), wind speed (u_2 at 2 meters), and relative humidity (RH), which are fundamentally unavailable for the early 20th-century historical reference period used in our synthetic reconstruction.

Crucially, this methodological constraint introduces a significant conservative bias into our findings. The localized Foehn effect generates exceptionally strong, dry katabatic winds that substantially elevate actual evapotranspiration by constantly removing the thin layer of humid air directly above the evaporating surfaces. Concurrently, the adiabatic warming drastically lowers RH. Because temperature-only models fail to account for the aerodynamic transport of moisture by these high-velocity winds, they systematically underestimate the true evaporative demand of the Xerokampos enclave. Thus, the classification of the area as marginally satisfying the BWh threshold via Thornthwaite and Holdridge is considered a highly robust lower-bound estimate; the actual, field-level aridity index is undoubtedly even more pronounced, placing it deeper into the true desert spectrum.

4.3 Ecophysiological Implications of the BWh Microclimate

The mathematical classification of Xerokampos as a Hot Desert (BWh) microclimate is beautifully mirrored by its localized ecology. The severe limitations on available water resources impose a strict environmental filter, dictating distinct ecophysiological survival strategies. The native flora, particularly the

Table 3: Application of Bioclimatic Indices for Xerokampos, Lasithi (Summary Classification)

Bioclimatic Index	Data / Calculation	Climate Classification
UNEP [Holdridge]	$AI = 219.5/1,231.6 = \mathbf{0.178}$	**Arid (Desert)**
UNEP [Thornthwaite]	$AI = 219.5/1,100.5 = \mathbf{0.199}$	**Arid (Desert)**
Holdridge System	$PET = \mathbf{1,231.6}$ mm	**Subtropical Desert Scrub**
Köppen (Synthetic)	171.2 mm < 209.0 mm	**BWh (Hot Desert)**
Köppen (Contemporary)	219.5 mm ≈ 209.0 mm	**BSh (marginal BWh)**
De Martonne [Contemp.]	219.5 mm : $I = 7.10$	**Arid**
De Martonne [Synth.]	171.2 mm : $I = 5.54$	**Arid (marginal Absolute Desert)**
De Martonne [Hist.]	148.7 mm : $I = 4.81$	**Absolute Desert**

isolated populations of African taxa, exhibit classical xerophytic and halophytic adaptations.

The extensive root architectures of these plants are designed to penetrate deep into the rocky limestone substrate to access hidden, deep-seated moisture reserves that escape the extreme surface evaporation. Above ground, adaptations such as microphylly (small leaves), seasonal leaf shedding during the peak of the summer drought, and the development of dense, waxy cuticles serve to drastically reduce transpirational water loss. Furthermore, the topography creates an endorheic-like coastal salt pan (Alatsolimni), where high evaporation rates concentrate soil salinity. This combination of intense solar radiation, extreme vapor pressure deficit, and high soil salinity creates a compound stress environment. The ability of this specific biome to not merely survive, but form a stable, climax community in these conditions, offers compelling biological validation of the mathematical models asserting a localized desert regime.

5 Model Validation

5.1 Cross-validation and RSR stability

To test reliability, the contemporary time series was divided into sub-periods (p). The rain shadow ratio (RSR_p) was calculated as:

$$RSR_p = \left(\sum_{i \in p} P_{\text{Xero},i} \right) / \left(\sum_{i \in p} P_{\text{Ref},i} \right) \tag{10}$$

The analysis of the "wet" period 2020-2022 (Avg. 330.1 mm) and the arid period 2023-2025 (Avg. 119.4 mm) shows that the rain shadow mechanism remains structurally active, with the divergence widening significantly during dry periods. This indicates that under drought conditions, the orographic suppression of rainfall becomes even more absolute.

5.2 Statistical Validity and Regression Diagnostics

To ensure the temporal stationarity and predictive validity of the Rain Shadow Ratio (RSR), rigorous statistical diagnostics were applied to the overlapping observation period against Toplou Monastery (n=76 months). A simple linear regression analysis between the reference station and the studied enclave yielded a strong positive correlation ($r = 0.76$, $p < 0.001$). The coefficient of determination ($R^2 = 0.58$) indicates that 58% of the precipitation variance in Xerokampos is explained by the broader regional synoptic patterns recorded by the reference station, as strictly moderated by the orographic barrier. Furthermore, to quantify uncertainty, a 95% Confidence Interval (CI) was calculated via 10,000 Bootstrap iterations for the baseline RSR, establishing $RSR = 0.719 \pm 0.15$.

5.3 Independent Verification and Errors

Validation using the aforementioned correlation structure from Toplou Monastery yielded high accuracy indices:

$$MAE = \frac{1}{N} \sum_{i=1}^{N} |P_{\text{obs},i} - P_{\text{est},i}| = \mathbf{10.0\,mm} \tag{11}$$

$$RMSE = \sqrt{\frac{1}{N} \sum_{i=1}^{N} (P_{\text{obs},i} - P_{\text{est},i})^2} = \mathbf{16.9\,mm} \tag{12}$$

The remarkably narrow confidence envelope confirms that the rain shadow mechanism constitutes a stable structural characteristic rather than a stochastic artifact of observational error.

5.4 Regional Verification and Precipitation Triangulation

To further fortify the results and exclude localized statistical error, a spatial precipitation triangulation was performed with the most arid official stations of the South Aegean: Karpathos (HNMS, 2026, reference climate period 1996-2026, $P = 292.4$ mm) and Kasos (NOA, 2026, 2010-2026, $P = 254.2$ mm). The Rain Shadow Ratio (RSR) of Xerokampos ($P = 219.5$ mm) against the two independent aridity proxies is calculated as follows:

$$RSR_{\text{Karpathos}} = \frac{P_{\text{Xerokampos}}}{P_{\text{Karpathos}}} = \frac{219.5}{292.4} = \mathbf{0.75} \tag{13}$$

$$RSR_{\text{Kasos}} = \frac{P_{\text{Xerokampos}}}{P_{\text{Kasos}}} = \frac{219.5}{254.2} = \mathbf{0.86} \tag{14}$$

These data indicate strong climatic differentiation even among the driest zones: Xerokampos systematically records 25% less

Table 4: Comparative Analysis of Extreme Aridity Indicators: ERA5 vs. In-Situ Observations

Climate Parameter / Period	ERA5	In-Situ Data	Deviation (Δ) & Climatic Interpretation
Current Period (01/2020-03/2026)	MAP: **212.0 mm**	MAP: **219.5 mm**	$\Delta = -7.5$ mm. The corrected methodology confirms the severe precipitation deficit of the enclave.
Absolute Minimum Annual Precip.	126.2 mm (Year 1955)	99.8 mm (Year 2023)	In-situ measurements capture extreme arid conditions ($<$100 mm) that the macroscopic grid fails to fully resolve.
Extreme 3-Year Drought (01/2023-12/2025)	MAP: 159.8 mm/yr	MAP: 119.4 mm/yr	$\Delta = -40.4$ mm (-25%). Strong indication of the virga effect due to Foehn winds.
Intra-decadal Climate Shift (2020-22 vs 2023-25)	Drop: 264.9 mm to 159.8 mm (-40%)	Drop: 330.1 mm to 119.4 mm (-64%)	Local stations record a more intense climatic transition compared to the moderated marine models.
Longest Continuous BWh Phase ($<$209 mm)	02/2004-12/2018 (179 months / approx. 15 yrs)	N/A (Start 2020)	MAP: 208.02 mm. Long-term gridded data confirm the structural capacity for a prolonged Hot Desert (BWh) climate.

precipitation than the extremely arid Karpathos station (BSh) and 14% less precipitation than marginally arid Kasos. The mathematical scaling of Xerokampos, maintaining the structural ratios, estimates the long-term precipitation of the area at 219.3 mm (via Karpathos) and at 218.6 mm (via Kasos).

5.5 Validation via Gridded Data and Spatial Resolution Constraints

To further evaluate the localized climatic anomaly and mitigate potential instrumental uncertainties, an independent methodological verification was conducted using the ERA5 global atmospheric reanalysis dataset (ECMWF; Hersbach et al., 2020). While global climate models and reanalysis products provide robust macro-scale atmospheric data, their application in topographically complex coastal regions is frequently constrained by inherent grid spatial resolution limits. Specifically, the ERA5-Land dataset operates at a spatial resolution of $0.1^\circ \times 0.1^\circ$ (approximately 9 km).

When querying the exact coordinates of the Xerokampos meteorological station (35.052°N, 26.240°E), the corresponding model grid cell inevitably encompasses a significant portion of the adjacent elevated terrain of the Ziros massif. This spatial aggregation is a known flaw of gridded datasets operating over steep coastlines; it results in a mathematical averaging of the arid coastal strip with the wetter, higher-altitude inland slopes. The model effectively "smooths" the mountain into the sea, leading to a systematic overestimation of local coastal precipitation and an inherent inability to accurately resolve the microclimate characterizing the immediate shoreline.

To mitigate the profound orographic bias introduced by this spatial blending and to isolate the thermodynamic impact of the Foehn effect without terrestrial contamination, a targeted data extraction strategy was applied. Data were retrieved from the standard ERA5 single-levels reanalysis dataset at an adjacent, purely marine grid point situated offshore (35.00°N, 26.25°E). This specific cell was selected to represent the undisturbed marine atmospheric boundary layer, capturing the baseline precipitation potential of incoming air masses over the open Libyan Sea, completely free from continental orographic influences and the associated land-sea mask interpolation errors.

The temporal window for this extraction was strictly aligned with the operational period of the in situ Davis station (January 2020 to March 2026) to ensure temporal consistency in the comparative analysis. To address the seasonality bias associated with non-integer years in the 2020-2026 series, the monthly weighted average method (extraction of mean value per month) was applied. This rigorous approach yielded a Mean Annual Precipitation (MAP) of **212.0 mm**.

The intra-annual distribution of this simulated marine precipitation demonstrated a pronounced dry season, with minimal to zero precipitation during the summer months (e.g., 0.0 mm in July, 0.7 mm in August), in absolute agreement with broader regional Mediterranean dynamics. When compared to the in situ measurements recorded at the Xerokampos terrestrial station, which indicate a MAP of 219.5 mm, an exceptionally marginal difference of only **7.5 mm** is observed. This close statistical alignment between the undisturbed offshore marine baseline (**212.0 mm**) and the coastal measurements (219.5 mm) provides compelling evidence supporting the presence of a severe rain shadow effect.

The data robustly suggest that despite its location on the continental landmass, the immediate coastal zone of Xerokampos experiences an atmospheric precipitation regime directly analogous to that of the open sea. This observation is flawlessly consistent with the thermodynamic hypothesis that the Ziros orographic barrier effectively shields the coastal enclave from moisture-bearing inland systems. As air masses descend the leeward slopes, they undergo significant dry adiabatic warming, accelerating the evaporation of vertically descending hydrometeors (virga) prior to surface impact. Consequently, this comparative analysis underscores the critical importance of high-resolution in situ monitoring in complex topographies, as subgrid scale microclimatic features—such as this highly localized arid biome—remain largely unresolved by macroscopic grid interpolations and standard global reanalysis products.

5.6 Long-term Climate Normalization (1996-2026)

To establish a robust climatic baseline and adhere to the World Meteorological Organization (WMO) standards for climate nor-

mals, a 30-year longitudinal analysis was conducted, spanning from April 1996 to March 2026. Data were synthesized from the ERA5 offshore reanalysis grid point ($35.00°\text{N}, 26.25°\text{E}$) to ensure a continuous and homogeneous time series. The analysis yielded a Mean Annual Precipitation (MAP) of **227.1 mm**. This long-term average demonstrates a high degree of convergence with contemporary in situ measurements (219.5 mm), representing a minimal difference of approximately 3.4%. The stability of the precipitation deficit over a three-decade period provides compelling evidence that the aridity of Xerokampos is not a transient meteorological event or the result of a decadal drought cycle. Rather, it constitutes a permanent, structural microclimatic feature. The multi-decadal verification reinforces the classification of the region as transitional from semi-arid to desert climate and highlights the status of the area as a stable arid biome within the climatic context of the South Aegean.

5.7 Computational Analysis of Extreme Aridity Periods

An exhaustive computational window-search within the 30-year reanalysis dataset identified continuous periods where Xerokampos structurally satisfies the Hot Desert (BWh) criteria. A continuous 15-year period (Feb 2004 - Dec 2018) recorded a MAP of **208.02 mm**, strictly falling below the desertification threshold. Furthermore, the last decade (May 2015 - November 2025) shows an intensification of aridity, with a MAP of **200.18 mm**. It should be noted that the ERA5 dataset, while providing a robust marine baseline, may underestimate the true magnitude of the local rain shadow phenomenon. In situ observations from the Xerokampos station suggest even more intense arid conditions, as reanalysis products often aggregate sub-grid thermodynamic processes. Consequently, terrestrial precipitation amounts are likely even lower than the presented reanalysis values.

5.8 Multi-decadal Comparative Regional Analysis from ERA5 (1940-2026)

A multi-decadal comparative analysis (1940-2026) reveals a persistent aridity gradient along the 35th parallel in the Libyan Sea, where Xerokampos exhibits the lowest precipitation levels in Greece, recording a 9.5% decrease in the recent 30-year period, with the local coastal zone exceeding the desertification threshold (209 mm) in a proportion ranging from 24% to 28% of the century's years. In contrast to the islands of the central and southern Aegean (e.g., Santorini, Kasos, Karpathos), which experience desert conditions only occasionally (1-8%) when evaluated based on their respective temperature-adjusted thresholds, the coastal zone of the southeastern Libyan Sea functions as a stable arid enclave, a fact further corroborated by the unique historical minimum of 1955, which distinguishes its climatic regime from the rest of the Aegean.

5.9 Sensitivity Analysis of RSR to Synoptic Conditions

To test the hypothesis of the spatial and temporal stability of the RSR ratio, a sensitivity analysis was conducted regarding different synoptic weather types, utilizing selected extreme episodes from the 2020-2026 period. The interaction between regional weather fronts and local topography dictates the daily precipitation outcomes. During February 2026, a period dominated by a sustained West-Southwest (WSW) atmospheric stream, the orographic blocking from the Ziros massif was maximized due to the specific angle of attack. The calculation of the local RSR ratio against the two reference stations was shaped as follows:

$$\begin{aligned} RSR_{\text{Ierapetra (WSW)}} &= \frac{25.5\,\text{mm}}{62.8\,\text{mm}} = \mathbf{0.41} \\ RSR_{\text{Toplou (WSW)}} &= \frac{25.5\,\text{mm}}{44.8\,\text{mm}} = \mathbf{0.57} \end{aligned} \tag{15}$$

However, the most striking dynamic of the orographic cutoff emerged during the examination of a historically unprecedented major system in September 2023 (Medicane/Storm Daniel). This system was characterized by a severe and persistent North-Northwest wind stream, establishing a powerful Omega block over the Mediterranean. While central Greece received catastrophic rainfall, eastern Crete experienced a strong northerly flow. During this specific episode, Toplou Monastery (situated on the exposed northern coast) recorded 64.6 mm of precipitation. In drastic contrast, Xerokampos was limited to a negligible 3.6 mm. The calculation of the ratio (RSR Toplou) for this specific, highly energetic episode yields the following extreme proportion:

$$RSR_{\text{Toplou (Daniel)}} = \frac{3.6\,\text{mm}}{64.6\,\text{mm}} = \mathbf{0.055} \tag{16}$$

The fact that Xerokampos received merely 5.5% of the precipitation of the windward side during a massive cyclonic event highlights the nearly absolute shielding of the enclave by the local topography under northern directions. The air masses were entirely depleted of moisture upon crossing the Ziros heights. These extreme fluctuations indicate that, although the RSR varies depending on the specific synoptic conditions and the trajectory of incoming fronts, the rain shadow mechanism remains structurally active and dominant. It reaches its maximum intensity (resulting in near-zero precipitation) during the prevalence of the northern sector, effectively nullifying the impact of regional storms.

5.10 ERA5 Grid Sensitivity Analysis and Orographic Elevation Bias

To further examine the orographic bias in low-resolution global climate models, a sensitivity analysis was performed between the marine and terrestrial ERA5 grids. Data extraction for the terrestrial cell ($35.05°\text{N}, 26.24°\text{E}$) yielded a MAP of 354.3 mm (1996-2026). This significant overestimation is attributed to the fact that the ERA5 model recognizes this specific point at a mean elevation of 753 meters, essentially incorporating the Ziros mountain massif with the coastal zone. The Absolute Orographic Bias ($\Delta P_{\text{onshore}}$) and the Overestimation Factor (OOF) are calculated as follows:

$$\begin{aligned} \Delta P_{\text{onshore}} &= MAP_{\text{onshore}} - MAP_{\text{in-situ}} \\ &= 354.3\,\text{mm} - 219.5\,\text{mm} = +\mathbf{134.8}\,\text{mm} \end{aligned} \tag{17}$$

$$OOF = \frac{MAP_{\text{onshore}}}{MAP_{\text{in-situ}}} = \frac{354.3}{219.5} = \mathbf{1.61} \tag{18}$$

Table 5: Comparative Analysis of Multi-decadal Precipitation and Aridity Thresholds from ERA5 (1940-2026)

Location	30-yr MAP (1996-2026)	Historical MAP (1940-2026)	Historical Drop	BWh Threshold	Desert Years (%)	Longest BWh Phase	Driest Year	Wettest Year
Xerokampos	227.1 mm	251.0 mm	-9.5%	209 mm	21 / 86 (24.4%)	02/2004-12/2018 (14.9 yrs)	126.2 (1955)	392.1 (1972)
Anafi	278.2 mm	306.6 mm	-9.3%	191 mm	5 / 86 (5.8%)	03/2022-11/2025 (3.8 yrs)	169.5 (1990)	563.0 (2019)
Kasos	286.5 mm	308.9 mm	-7.2%	200 mm	6 / 86 (7.0%)	03/2004-11/2008 (4.8 yrs)	159.5 (1990)	480.7 (2019)
Anavyssos	293.9 mm	296.9 mm	-1.0%	191 mm	7 / 86 (8.1%)	04/1998-10/2001 (3.6 yrs)	138.0 (2000)	541.8 (2003)
Karpathos	296.8 mm	316.3 mm	-6.2%	198 mm	3 / 86 (3.5%)	02/2004-11/2007 (3.8 yrs)	162.1 (1989)	481.0 (2019)
Santorini	299.5 mm	328.6 mm	-8.9%	191 mm	2 / 86 (2.3%)	04/2022-11/2025 (3.7 yrs)	180.4 (1990)	566.7 (1968)
Ios	336.9 mm	373.4 mm	-9.8%	191 mm	1 / 86 (1.2%)	03/1988-10/1990 (2.7 yrs)	174.3 (1989)	732.1 (1968)

Conversely, the selection of the marine cell $(35.00°\mathrm{N}, 26.25°\mathrm{E})$, which is correctly recognized at zero elevation (0m), minimizes the deviation to +7.6 mm against the 30-year baseline (227.1 mm).

5.11 Multi-decadal Quantification of the Virga Effect (1940-2026)

The extension of the analysis over 86 years (1940-2026) allows for the direct quantification of the atmospheric water resource loss. Comparing the historical data of the two cells reveals a stable thermodynamic deficit (V_{virga}):

$$\begin{aligned} V_{\text{virga}} &\approx MAP_{\text{onshore (753m)}} - MAP_{\text{offshore (0m)}} \\ &= 391.6\,\text{mm} - 251.0\,\text{mm} = \mathbf{140.6}\,\text{mm/yr} \end{aligned} \tag{19}$$

This difference acts as a mathematical proxy of the volume of vertical hydrometeors evaporating in mid-air (virga effect) due to the dry adiabatic heating of the Foehn katabatic winds, before they can reach the surface of the coastal enclave.

6 Limitations and Uncertainty Analysis

The present study inherently acknowledges that the contemporary time series derived from the local Davis weather station (n=7 years) falls short of the rigorous 30-year climate reference period explicitly defined by the World Meteorological Organization (WMO) for establishing climatological standard normals. Short-term data are inherently susceptible to decadal oscillations and transient synoptic anomalies. Furthermore, instrumental limitations must be considered; unshielded tipping-bucket rain gauges in areas prone to high-velocity winds (such as the Foehn gusts in Xerokampos) may suffer from aerodynamic undercatch, potentially exaggerating the recorded precipitation deficit by a small margin.

However, the strategic use of the Synthetic Climate Reconstruction (n=22 years) paired with the long-term ERA5 reanalysis and the robust statistical validation of the Rain Shadow Ratio (RSR) mitigate these temporal constraints. The convergence of these independent methodologies indicates that the observed aridity is not a statistical artifact of a recent drought cycle, but rather constitutes a profound structural characteristic dictated by the immutable local geomorphology. The Ziros orographic barrier acts as a permanent thermodynamic regulator, ensuring the perpetual continuity of the Foehn mechanism. Finally, the marginal classification (219.5 mm) against the strict hot desert threshold (209.0 mm) makes the results highly sensitive to minor variations in input data, underscoring the absolute necessity for continuous, long-term monitoring and potentially the future deployment of eddy covariance towers to directly measure the latent heat fluxes in this extreme environment.

7 Conclusions

This study provides consistent multi-method evidence that the coastal enclave of Xerokampos (Lasithi, Crete) constitutes an exceptional case of localized climatic aridity within the Mediterranean basin. The convergence of in-situ observations (MAP = 219.5 mm), synthetic reconstruction (171.2 mm), and ERA5 offshore reanalysis (227.1 mm, 30-year normal) indicates a persistent and recurrent precipitation deficit.

The close agreement between offshore marine precipitation ($\sim$212 mm for 2020--2026) and terrestrial station measurements suggests that the coastal zone approaches a precipitation regime analogous to the adjacent open sea, indicating strong orographic suppression of rainfall. This behavior is physically consistent with a pronounced rain shadow effect induced by the Ziros massif, combined with dry adiabatic warming and enhanced sub-cloud evaporation (virga) associated with Foehn-type katabatic flows.

Bioclimatic classification indices place the region at or near the arid regime threshold. The UNEP Aridity Index ($AI = 0.178$--0.199) indicates conditions at or marginally below the desert boundary, while the De Martonne Index ($I = 5.5$--7.1) supports a classification ranging from arid to marginal absolute desert under synthetic scenarios. The Köppen-Geiger classification, when applied to reconstructed and long-term datasets, suggests a transitional BSh--BWh climatic regime, with multi-decadal periods satisfying the strict Hot Desert (BWh) threshold.

Despite the relatively short duration of the contemporary in-situ record (2020--2026), the consistency across independent datasets and the stability of the Rain Shadow Ratio (RSR), supported by statistical validation and regional triangulation, indicate that the observed aridity is not a transient anomaly but a persistent microclimatic feature controlled by local topography.

It is important to note that the evapotranspiration estimates employed in this study are based on temperature-driven empirical models (Holdridge, Thornthwaite), which likely underestimate the true atmospheric demand under strong Foehn conditions. Therefore, the presented aridity indices should be interpreted as conservative lower-bound estimates.

Overall, the findings support the interpretation that Xerokampos represents a highly localized, topographically controlled arid enclave, functionally approaching desert-like conditions within the southeastern Mediterranean. However, given the marginal

proximity to classification thresholds and inherent methodological uncertainties, the region is most appropriately described as a borderline desert microclimate rather than a fully developed zonal desert climate.

References

Barry, R. G., & Chorley, R. J. (2009). *Atmosphere, weather and climate* (9th ed.). Routledge.

Beck, H. E., Zimmermann, M. E., McVicar, T. R., Vergopolan, N., Berg, A., & Wood, E. F. (2023). Present and future Köppen-Geiger climate classification maps at 1-km resolution. *Scientific Data, 10*, 628.

De Martonne, E. (1926). Aréisme et indice d'aridité. *Comptes Rendus de l'Académie des Sciences, 182*, 1395-1398.

Demetrakos, D. B. (1950). *Mega lexikon tis Ellinikis glossis*. Archaios Ekdotikos Oikos.

Eig, A. (1931). Les éléments et les gruppi phytogéographiques auxiliaires dans la flore palestinienne. *Repertorium Specierum Novarum Regni Vegetabilis, Beihefte, 63*, 1-201.

Emberger, L. (1955). Une classification biogéographique des climats. *Recueil des Travaux des Laboratoires de Botanique, Géologie et Zoologie de la Faculté des Sciences de l'Université de Montpellier, 7*, 3-43.

Flocas, A. A., & Bloutsos, A. A. (1991). Aridity over Greece. *Climatological Bulletin, 25*(2), 101-107.

Hellenic National Meteorological Service (HNMS). (2026). *Climatological database*. `http://oldportal.emy.gr/emy/en/climatology/climatology`

Hersbach, H., Bell, B., Berrisford, P., Hirahara, S., Horányi, A., Muñoz-Sabater, J., ... & Thépaut, J. N. (2020). The ERA5 global reanalysis. *Quarterly Journal of the Royal Meteorological Society, 146*(730), 1999-2049.

Holdridge, L. R. (1947). Determination of world plant formations from simple climatic data. *Science, 105*(2727), 367-368.

Holdridge, L. R. (1967). *Life zone ecology*. Tropical Science Center.

Kotroni, V., Lagouvardos, K., Bezes, A., Dafis, S., Galanaki, E., Giannaros, C., Giannaros, T., Karagiannidis, A., Koletsis, I., Kopania, T., Papagiannaki, K., Papavasileiou, G., Vafeiadis, V., & Vougioukas, E. (2020). The METEO.GR observing network of the National Observatory of Athens. *Bulletin of the American Meteorological Society, 101*(4), E373-E383.

Lionello, P., Malanotte-Rizzoli, P., & Boscolo, R. (Eds.). (2006). *Mediterranean climate variability*. Elsevier.

Magarey, R. D., Borchert, D. M., & Schlegel, J. W. (2008). Global plant hardiness zones for phytosanitary risk analysis. *Scientia Agricola, 65*(1), 54-59.

Mariolopoulos, E. G. (1938). *The climate of Greece*. Tarousopoulos Printing.

Mass, C. F., Ovens, D., Westrick, K., & Colle, B. A. (2002). Does increasing horizontal resolution produce more skillful forecasts? *Bulletin of the American Meteorological Society, 83*(3), 407-430.

Municipality of Sitia. (2024). *Biodiversity declaration*. Retrieved from `https://sitia.gr/wp-content/uploads/2024/08/diakiryxi_biopoikilotitas.doc`

Nastos, P. T., & Zerefos, C. S. (2009). Spatial and temporal variability of precipitation over Greece. *Global and Planetary Change, 69*(1-2), 58-67.

National Observatory of Athens (NOA). (2026). *Monthly Climate Bulletins*. `https://www.meteo.gr/Monthly_Bulletins.cfm`

Nobel, P. S. (1994). *Remarkable agaves and cacti*. Oxford University Press.

Peel, M. C., Finlayson, B. L., & McMahon, T. A. (2007). Updated world map of the Köppen-Geiger climate classification. *Hydrology and Earth System Sciences, 11*(5), 1633-1644.

Rackham, O., & Moody, J. (1996). *The making of the Cretan landscape*. Manchester University Press.

Sevruk, B., Ondráš, M., & Chvíla, B. (2009). The WMO precipitation measurement intercomparisons. *Journal of Geophysical Research: Atmospheres, 114*(D8).

Sitia UNESCO Global Geopark. (2026). *Koufonisi and Kavalloi islets*. `https://sitia-geopark.gr/the-region.aspx`

Szelepcsényi, Z., Breuer, H., & Sümegi, P. (2014). Application of the Holdridge life zone system to the present and future climate of Europe. *Időjárás, 118*(1), 69-82.

Thornthwaite, C. W. (1948). An approach toward a rational classification of climate. *Geographical Review, 38*(1), 55-94.

Tsanis, I. K., Koutroulis, A. G., Daliakopoulos, I. N., & Jacob, D. (2011). Severe climate-induced water shortage and extremes in Crete. *Climatic Change, 106*(4), 667-677.

Turland, N. J., Chilton, L., & Press, J. R. (1993). *Flora of the Cretan area: Annotated checklist and atlas*. HMSO.

Türkeş, M. (1999). Vulnerability of Turkey to desertification with respect to precipitation and aridity conditions. *Turkish Journal of Agriculture and Forestry, 23*(4), 363-380.

United Nations Environment Programme. (1992). *World atlas of desertification*. Edward Arnold.

Vrochidou, A. E. K., Tsanis, I. K., Grillakis, M. G., & Koutroulis, A. G. (2013). The impact of climate change on hydrometeorological droughts at a basin scale. *Journal of Hydrology, 476*, 290-301.

Warner, T. T. (2010). *Numerical weather and climate prediction*. Cambridge University Press.

Whiteman, C. D. (2000). *Mountain meteorology: Fundamentals and applications*. Oxford University Press.

Xerokampos Weather Station. (2026). *Xerokampos Lasithi meteorological data archive (Davis Instruments)* [Data set]. `https://www.xerocamboscreta.com/dati-mensili.html`

Xoplaki, E., González-Rouco, J. F., Luterbacher, J., & Wanner, H. (2004). Wet season Mediterranean precipitation variability: Influence of large-scale dynamics and trends. *Climate Dynamics, 23*(1), 63-78.

Zohary, M. (1973). *Geobotanical foundations of the Middle East*. Gustav Fischer Verlag.